CHAPTER 2

DETECTION OF EMPTY WAVES

QuWT-c2-220503

Historically, the detection of presumptively empty discrete wave packets has been problematic. Methods other than those described here have been used to generate such presumptively empty waves. These methods commonly use a beam splitter to divide an incident discrete photon into two paths. If a detector placed on one path measures an energy quantum, an empty wave packet should then still be propagating on the other path if such real entities exist.

That empty wave of a photon, if real, should be able in principle to cause a measurable effect on the occupied wave of the photon. An ingenious method for demonstrating such an effect was proposed by Croca et al. [318]

However, reported experiments designed to detect these presumptively empty discrete wave packets have not yielded conclusive evidence of their existence. It is certainly not unreasonable to expect a similar difficulty in detecting the discrete empty wave packets generated by the polarization methods described here which also portends a limited utility for those discrete empty wave packets.

2.1 TRANSITION TO SINGLE LONGITUDINAL MODE COHERENT BEAMS

Both of these impediments, problematic detectability and limited utility, are counterintuitively resolved by using a linearly polarized coherent single longitudinal mode SLM source in place of a linearly polarized discrete photon source. In the optical regime, properly configured lasers can generate such SLM beams.

A coherence length of a linearly polarized SLM beam is analogous to a discrete linearly polarized photon in several respects. Longitudinally, both are represented by a coherent wave structure. Individual photons extracted from an SLM coherence length, i.e. a single mode, have indistinguishable polarizations, e.g [350]. Consistent with LR, this indistinguishability implies that the entire SLM coherence length has some particular orientation θ in

analogy to the wave packet of a linearly polarized discrete photon. Linearly polarized SLM beams and linearly polarized discrete photon beams both exhibit polarization ensemble orientation distributions. That is, statistically each of the sequentially emitted linearly polarized SLM coherence lengths has an orientation θ that is in accord with a random member of a polarization ensemble as is the case for linearly polarized discrete photons. From these analogous properties of linearly polarized SLM beams and linearly polarized discrete photon beams it can be deduced that the described methods for generating discrete empty wave packets also generates sequential coherence lengths of single mode empty waves.

Notably, it is the differences between SLM beams and discrete photon beams that yield the means for providing the detectability and utility of empty waves. An SLM coherence length is commonly extraordinarily longer than a corresponding discrete photon wave packet. In the optical regime a coherence length on the order of tens of meters is not unusual. Additionally, wave intensity on an SLM coherence length is typically many, many orders of magnitude higher than that of a discrete photon because of the density and multitude of photons on the former collectively contributing to that wave intensity.

In order to quantify the intensity of the empty coherence lengths extracted from the incident SLM coherence lengths we must statistically compute the average of individual member $W=\sin^2\theta$ values over a polarization ensemble distribution of θ orientations. The intensity of any emitted coherence length is randomly dependent upon the particular ensemble member orientation θ associated with a given SLM coherence length incident on the polarizer. That computed average is $\langle\sin^2\theta\rangle\approx 0.11$ (more precisely, 0.1073). Then, with the incident SLM coherence length intensity normalized to unity, the individual sequential empty coherence lengths have an ensemble distribution of $W=\sin^2\theta$ intensities and an ensemble averaged W=0.11.

As a practical matter, a mere several dozen or so sequential empty wave coherence lengths could be used to represent a digital “1” pulse. That pulse would have an average wave intensity (probability flux density) closely approximating W=0.11. If that empty wave pulse is transmitted to a distant receiver where it is fully “restored” to an ordinary energy-bearing pulse, it

would have an irradiance (energy flux density) I that is ≈11% as large as that of the initial ordinary energy-bearing SLM source beam.

2.2 UNITS

For various considerations presented here both theoretical and experimental, it very useful to readily translate beam parameters between different sets of units. The intrinsic variables of irradiance “I” and wave intensity “W” are particularly useful in considering theoretical representations of beam parameters whereas the extrinsic variable of beam power is of practical use in experimental applications. Applied to Gaussian beams, the intrinsic variables commonly indicate their respective peak values along the beam as evaluated at the center of the beam cross section. Conversely, a detector intercepting a sufficiently large cross section of a beam that is inclusive of all significant irradiance, e.g. at a 1.5 Gaussian diameter, measures the extrinsic variable of the beam’s power (energy flux). In the optical regime that power for a laser beam is commonly be expressed in units such as Watts or milli-Watts.

Beams with very low divergence lend themselves to proportionate translations between intrinsic and extrinsic variables whereas along beams with significant divergence those intrinsic variables at the beam center significantly decrease as the beam diverges while the extrinsic variables are unchanged in value.

The above considerations have useful applications in the present context. For example, if a linearly polarized SLM laser beam has a power, energy flux, of one watt (Pwr=1000 mW), that extrinsic variable can be directly measured by a properly calibrated detector. If that beam is “ordinary,” i.e. has not been subjected to a process that would “deplete” or “enrich” its real particle-like (energy quanta E) aspect relative to its wave-like aspect, then that same detector measurement indirectly measures the “probability flux” of the beam.

Probability P is the quantum mechanical construct derived from integrated wave intensity where intensity is the squared modulus of the wave function amplitude. For an ordinary discrete photon wave packet, integration over that wave packet yields a unit probability since a unit observable energy quantum

resides on that wave packet. Effectively, the quantum mechanical formalism assigns proportionate and equal E=1 and P=1 as the extrinsic dimensionless variables associated with that discrete ordinary photon.

The extrinsic variables E and P can also be applied to a portion of some particular coherence length of a multi-photon beam. Integration of irradiance over that portion yields the inclusive energy quanta represented by E and a similar integration of intensity yields the inclusive probability P. For an ordinary beam, those extrinsic variables E and P can both be set equal to each other and, further, can be normalized to unity.

Nevertheless, as a practical matter in considering beam parameters in experimental configurations, extrinsic variables relating to power are of particular utility. Returning to the example of the ordinary linearly polarized SLM beam with an energy flux of 1000 mW, since the beam is ordinary we adapt the quantum mechanical formalism and set energy flux proportionate and numerically equal to probability flux. Then the beam's probability flux is represented here as 1000 mW-eq. In this adaptation the modifier "eq" is appended to energy flux units and represents the equivalent probability flux for an ordinary beam of some specified energy flux.

If that beam is incident on a polarizer, the energy flux I emitted by the polarizer's orthogonal axis ideally is zero. However, LR predicts that the horizontal axis output is an intensity (not irradiance) that is ~11% of the incident beam intensity. Consequently, that prediction translated to probability flux implies that a probability flux dP/dt=110 mW-eq is present on that orthogonal axis output.

If that empty, totally depleted, beam is transmitted to a remote receiver and transiently equilibrated with an ordinary high power "restoration" beam with Pwr>>1000 mW, that empty beam with a probability flux dP/dt=110 mW-eq is restored to an ordinary beam with Pwr=110 mW.

2.3 SLM vs MLM

In the optical regime, lasers are most commonly of the multi longitudinal mode MLM type, simultaneously emitting two or more distinct modes as opposed to an SLM laser which suppresses all but one mode in its cavity but is more difficult to construct. The respective distinct coherent modes of an MLM laser differ from each other by very small wave length increments so

that over an emitted coherence length the respective modes are substantially mutually in-phase. As the end of a coherence length is approached, the small wave length differences of the respective modes progressively degrade the in-phase condition to the point that there is mutual incoherence of the multiple modes at the end of a particular emitted coherence length.

If an MLM beam linearly polarized along 0° and comprised of N modes i=1 to N, is incident on a polarizer that has a 90° H polarization axis, the projections of each of those multiple modes yield an N-fold set of H outputs consisting of respective empty wave modes.

Any single "i^{th}" mode of a particular MLM coherence length comprised of the N modes i=1 to N has an orientation θ_i that is in accord with the orientation of a random member of a 0° polarization ensemble. Then, even for a relatively small N, the number of positive θ_i and negative θ_i will be approximately equal. Since the amplitudes of the H output empty waves are each modulated by respective $\sin\theta_i$ factors, the H output coherence length is characterized by approximately half of the empty wave modes being out of phase with the other half which results in poor restoration and detection. This deficiency does not occur with the use of an SLM source and for this, and other reasons, the use of an MLM source is suboptimal with regard to the utility of the generated empty waves.

2.4 EXPERIMENTAL DETECTION OF EMPTY WAVES

Fig. 2.1a shows the configuration that has provided a proof-of-principle demonstration for generating and detecting coherent empty waves in the optical regime. The general methodology for this configuration is examined in this section while a more detailed example of specific component and beam parameters is given in the subsequent section below.

A vertically (0°) polarized laser beam enters from the left. The beam is generated by a 10 mW 532 nm DPPS single longitudinal mode SLM laser with ~100:1 polarization and ~50 m coherence length. The beam is strongly attenuated by an initial neutral attenuator Attn-1 that provides a suitable low beam power for the digital photometer. At a 50:50 beam splitter BS-1, the transmitted fraction of the beam is intercepted by a chopper wheel CW producing pulses with a 50% duty cycle at 40 Hz. The pulsed beam is further

reduced by a second attenuator Attn-2 to control the power on the pulses relative to that on the beam fraction reflected at BS-1.

The pulsed beam is incident on a calcite polarizer POL that has a polarization axis horizontally (90°) oriented.

Various types of polarizers suitable for use in the apparatus may exhibit a polarization-independent attenuation factor in addition to the conventional polarization-dependent attenuation factor. That polarization-independent attenuation factor is subsumed here into Attn-2 for purposes of calculation.

For an ideal SLM source beam and polarizer, the pulses of the beam exiting the horizontal axis of Pol are comprised of empty waves, totally depleted of irradiance (energy quanta). The pulses have a wave intensity that is ~11% of the pulse wave intensity incident on Pol. As a practical matter, with non-ideal source beam polarization and non-ideal extinction value of the polarizer there is a small residual non-zero irradiance (and power) still present on the output pulse of Pol. That residual can be reduced to vanishingly small levels by the use of available source beams with improved polarization and polarizers with improved extinction. In any case the presence of that residual does not detract from the utility of the present apparatus in definitively demonstrating the restoration of a highly depleted beam. Moreover, a small readily measured residual power level on the pulse beam (in the absence of coupling with a restoration beam) provides a very useful baseline for accurately quantifying the relative restored beam power.

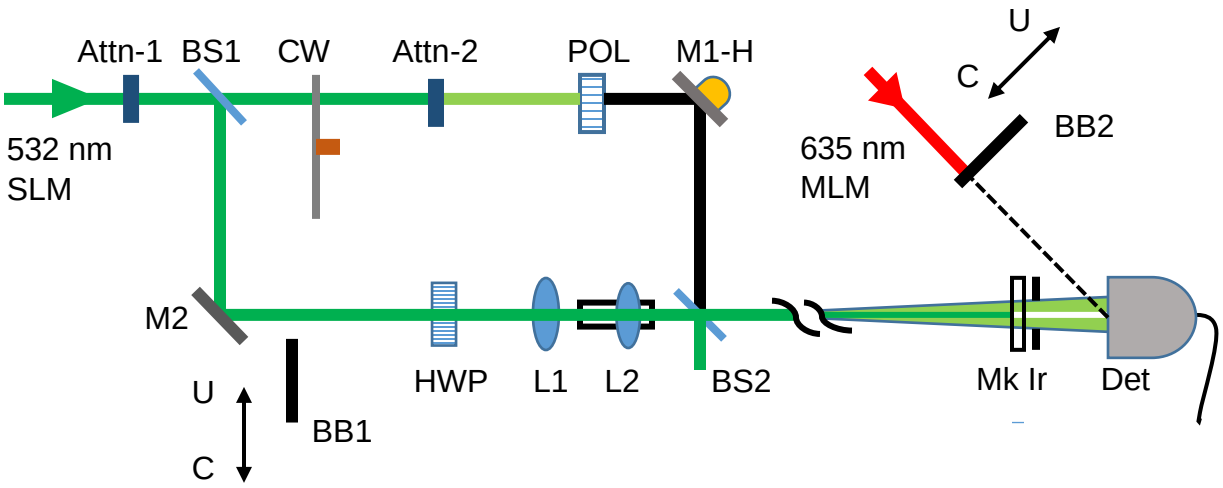

Fig's. 2.1a. Configuration of proof-of-principle demonstration for generating and detecting empty waves.

The (highly depleted) pulse beam is reflected by M1-H which consists of a mirror mounted on a beam director equipped with a haptic actuator. The haptic actuator is a compact motor-based oscillator in a 10 mm diameter, 2 mm thick enclosure that locally imparts a ~1K Hz vibration to the beam director. After reflection from M1-H, the highly depleted pulse beam is identified as the "signal beam" S. During pulse measurement that vibration removes the phase relation between the S beam and the beam fraction reflected at BS-1.

M1-H directs the pulse beam S is directed to a 50:50 beam splitter BS-2. The reflected fraction of S is directed over a ~1500 mm "coupling path" to mask plate MK that consists of a 2 mm diameter opaque mask centered on a glass substrate window. At Mk the Gaussian diameter of the pulse beam S as a result of natural divergence is approximately ~3 mm. Accordingly, with the pulse beam centered on the opaque mask, approximately 60% of the S beam's power on the coupling path is still transmitted through the Mk substrate window.

An iris Ir adjacent to Mk presents a ~3.5 mm aperture that blocks the peripheral S beam but still leaves ~40% of the S beam's original power on the coupling path incident on a PIN detector Det located just beyond Ir.

Concurrently, a fraction of the Attn-1 attenuated beam is reflected by beam splitter BS-1 to mirror M2. That beam fraction is identified as the “restoration beam” R. A two-position beam blocker BB-1 is located on the R beam path. When BB-1 is in position “C,” the R beam path is not blocked and beams S and R are coupled along the coupling path. Conversely, when BB-1 is in position “U,” the R beam path is blocked and is uncoupled from the S beam along the coupling path.

When the vertically polarized beam R continues beyond BB-1, it is incident on a zero order 532 nm quartz half wave plate HWP that rotates beam R to a horizontal polarization. Beam R then enters a two lens pair, lens L1 with a 25 mm focal length and lens L2 with a 100 mm focal length. A rail mounting of L2 permits a fine adjustment of the L1-L2 separation distance.

A fraction of the R beam is transmitted by beam splitter BS-2 with that R beam spot concentric to the S beam spot. Beams S and R are adjusted to be mutually concentric along the coupling beam path. Components Mk, Ir, and Det are aligned concentric to the coupling path.

The separation of the L1 and L2 lenses is adjusted to focus virtually all of the R beam power onto the mask Mk. The peripheral R beam power reaching the detector on the annular region between the mask and the iris should then be very approximately two orders of magnitude less than the R beam power blocked by the mask. Through that same annular region the residual S beam power and the R beam power are very approximately comparable. These relative powers are principally achieved by the choice of Attn-2 and advantageously contribute to minimizing the total dynamic range of critical pulse height measurement values.

The Fig. 2.1a configuration together with the exaggerated Fig. 2.1b detail depict the mechanism by which the S beam is transiently coupled to the R beam. Alternative restoration methods (ref coupling patent) provide higher coupling efficiency but the readily implemented present method is advantageous for a proof-of-principle demonstration.

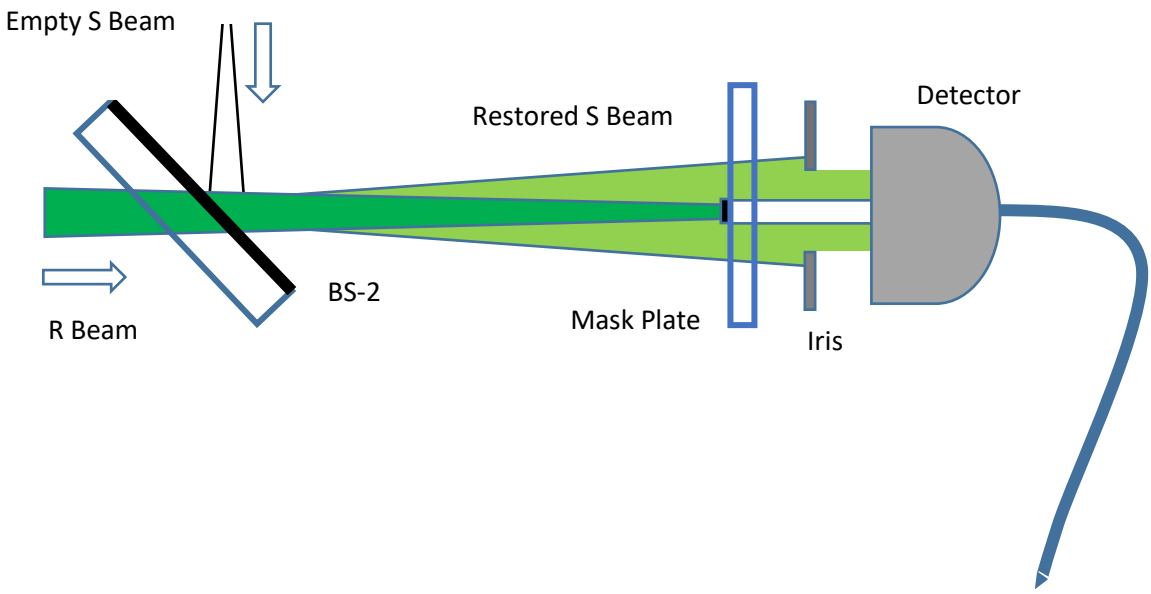

Figure 2.1b. Exaggerated, not-to-scale depiction of the beams on the coupling path and the adjacent components.

As the concentric beams leave BS-2 and enter the proximal region of the coupling path, the beam cross sections are still approximately equal. Along that proximal region the highly depleted S beam equilibrates with the initially ordinary $\Omega_{Ri}=1$ R restoration beam. That R beam is much more intense than the S beam, $W_R>>W_S$. As a result only a very small fraction of the R beam's initial coupling path irradiance I_{Ri} is transferred to the S beam as the beams propagate further along the proximal region of the coupling path and equilibrate to a final common $\Omega_f=\Omega_{Rf}=\Omega_{Sf}=I_{Rf}/W_R=I_{Sf}/W_S$ that is nearly unity as the beams approach the distal region of the coupling path. At this point the S beam is almost fully restored to an ordinary beam and both beams are very slightly depleted.

The proximal region of the coupling path substantially provides for the transient equilibration of the two beams. As those beams just begin to propagate onto the distal region of the coupling path, their respective occupation values remain at that common Ω_f. However, the nearly fully restored pulses of the S beam are not yet distinguishable from the R beam

because the increment of irradiance that restored those S beam pulses is absent on the R beam, leaving no net change of irradiance over the entire cross section of the two approximately equal diameter beams whether a pulse is present (and the S pulse has acquired that increment) or absent (and the increment still resides on R).

The remedy to that deficiency is provided as the two beams progress further along the coupling path well into the distal region. Because of lenses L1 and L2, the resultant convergence of the R beam relative to the S beam physically separates the two beams. Both beams still retain their common Ω_f but almost all of the R beam intensity is focused on a small central portion of the S beam cross section. That small central portion is blocked by a mask while leaving a still substantial annular region of the S beam incident on a detector. During a pulse, much of the increment of irradiance acquired by the S beam is on that annular region and is readily detected, but the concurrent loss of that increment from the R beam is not apparent at the detector because the R beam is almost entirely confined to a blocking mask.

In the intervening time intervals between the pulses the detector measures the substantially steady-state residual R beam irradiance “baseline” in the annular region. A digital oscilloscope receives the output signal of the detector amplifier and measures the signal difference between the pulse peaks and the intervening baseline. That difference constitutes the essential pulse height measurement Δ_C for the “C-mode” in which the S beam is coupled to the R beam shown in (c) of Fig’s. 2.1c-d. Since irradiance is an intrinsic variable, the collective areal increments of irradiance illuminating the detector properly constitute the extrinsic variable of power. By proper calibration Δ_C can then be expressed in power units such as milli-Watts.

In the absence of the R beam, a corresponding uncoupled U-mode pulse height Δ_U is similarly measured as depicted in (d) of Fig’s. 2.1c-d. For non-ideal circumstances, presumptively totally depleted (empty) unrestored S beam pulses may still exhibit some small non-zero residual irradiance on the detector. That residual irradiance may be measurable as an unrestored pulse peak level relative to the presumptively zero baseline level with R absent or a non-zero baseline level from a “bias” ancillary beam. In either case, the U-mode level differential can be expressed in power units and constitutes the essential pulse height measurement Δ_U.

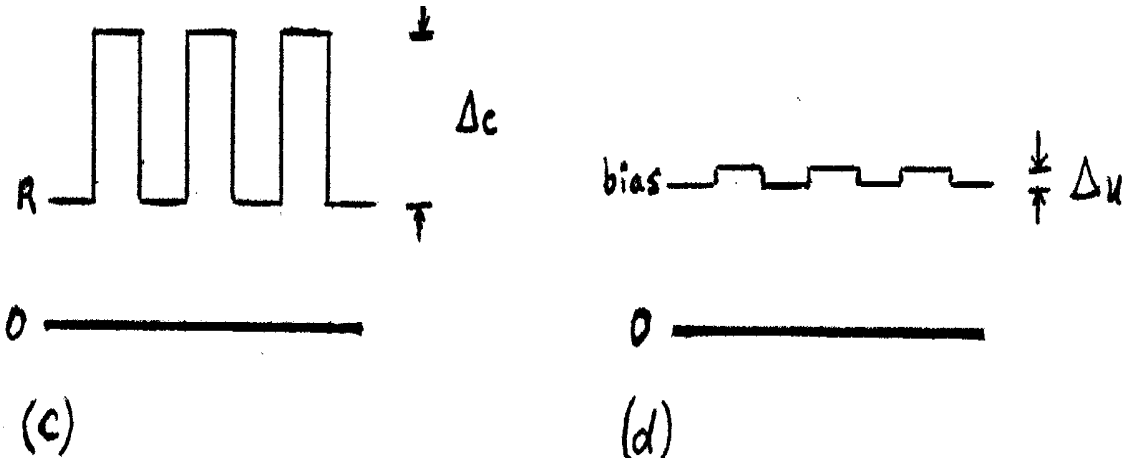

Figures 2.1c-d. Coupled-mode (c) shows restored S pulse heights on a baseline of residual R beam in annular region. Uncoupled-mode (d) depicts unrestored S pulse on an ancillary bias beam baseline.

If there is no significantly measurable value of Δ_U, the S beam is "empty" to within the limits of the measurement apparatus and concurrently Δ_C represents some measured value of power (energy flux), Pwr, restored onto that presumptively empty pulse. That restoration power Pwr then represents a probability (integrated intensity) flux of, at least, Pwr-eq if the pulse is fully restored to ordinary. That conclusion is consistent with the LR hypothesis that the occupation value for an ordinary beam Ω=Pwr/Pwr-eq=1 where Pwr and Pwr-eq are the complementary particle-like (energy quanta) and wave-like properties of a beam.

More commonly, Δ_U is a non-zero measurable value implying that the S beam pulses exiting Pol are not totally depleted. Concurrently, Δ_C represents some measured value of power (energy flux), Pwr, of presumptively fully restored pulses. That restoration power Pwr then represents the actual probability flux (integrated intensity) expressed as Pwr-eq consistent with the pulses being fully restored to ordinary. Because the presently considered Δ_U is a non-zero measurable value, the ratio $\Delta_U/\Delta_C=\Omega_{Si}$, where Ω_{Si} is the occupation value of the partially depleted S pulses before restoration.

Importantly, a demonstration of even a partial restoration to ordinary provides evidence of an $\Omega_{Si}<1$ in support of LR. Progressive improvements, typically in coupling path alignments, provide corresponding progressive reductions in the experimentally observed Ω_{Si} that converge to some minimum Ω_{Si}. That minimum Ω_{Si} is achieved when the coupling path fully

restores the pulses and potentially represents the actual non-zero occupation value of the S pulses exiting POL.

That small but actual non-zero Ω_{Si} can arise from several factors. Notable among these factors is the polarization of the linearly polarized SLM source beam. A modest but not untypical 100:1 polarization of that source can counterintuitively result in a significant departure of the actual Ω_{Si} from zero. For example, at 100:1, 1% of the source beam irradiance is transmitted at the POL's orthogonal axis. Concurrently, consistent with LR, ~11% of the source beam intensity is also emitted by that orthogonal axis as an empty wave. Together these emissions from the POL's orthogonal axis output predict an $\Omega_{Si}\approx 1\%/11\%\approx 0.09$. This Ω_{Si} can be reduced by various means, however for the purposes of refining a proof-of-principle demonstration, a non-zero Ω_{Si}, as a result of a non-zero Δ_U, provides a highly useful reference value in the process of optimizing coupling path alignments.

As a separate matter related to ensuring detector accuracy, a 635 nm MLM diode laser is used to provide an ancillary "bias" beam power on the detector that is approximately equal to that of the R beam as shown in Fig. 2.1d. A two-position beam blocker BB-2 is set in concert with BB-1. When both beam blockers are set to C, R is coupled to S and the bias beam path to the detector is blocked. Alternatively, when both are set to U, R is uncoupled from S and the bias beam is incident on the detector.

The ancillary beam ensures that detector samplings are acquired over a fully linear response range of the detector. A detector that nominally has a highly linear response may still exhibit a significant non-linear response at near-zero power levels. When operating in the uncoupled U-mode (with the R beam uncoupled from the detected S beam), an essential pulse height Δ_U is measured by a digital oscilloscope from the detector amplifier output. Δ_U is the differential between the peak level of the pulses and the steady-state baseline in the intervening time intervals between the pulses.

If an ancillary bias beam were not provided during this U-mode, there would be zero power present on the detector during those intervening time intervals and an accurate linear detector response might be in question. Conversely, if a steady-state ancillary bias beam power is provided on the detector, the baseline power is elevated away from the zero level, and during the presence of a pulse that bias power is simply additive to the pulse beam power since

the bias beam and the S beam are respectively at substantially non-interactive wavelengths. With that bias beam present the measurement of Δ_U is acquired without a problematic zero power level on the detector.

Similarly, as an additional separate matter, M1-Hp includes a haptic actuator to ensure that interference between S and R at the detector does not adversely affect the measurement of Δ_C. In the absence of a haptic actuator, the phase relation between S and R generates interference fringes at the plane of the detector. An excess or deficiency of bright fringes relative to dark fringes inclusive in the annular beam incident on the detector may result in a similar excess or deficiency of measured power in the Δ_C measurement. This potential source of error is eliminated by the use of the haptic actuator. The haptic actuator provides a 1 KHz vibration on that beam director and mirror that effectively removes any phase relation of the S beam with the R beam on the other leg of the apparatus configuration during the digital oscilloscope signal acquisition time. In order to maximize measurement accuracy in this proof-of-principle demonstration, the digital oscilloscope signal averages over 128 of the $1/40^{th}$ sec pulse cycles, i.e. 3.2 sec.

The haptic actuator is purposefully located on the “S” portion of the Fig. 2.1a configuration loop rather than the “R” portion because of the potential for highly destabilizing baseline excursions in the latter case. Virtually all of the highly intense convergent R beam is blocked from the detector by critical alignment on a small diameter mask leaving only a low intensity residual annular R beam on the detector. Any lateral disturbance of that alignment can produce a time-varying intense coronal leakage at an edge of the mask of the substantially blocked R beam.

The bias beam and haptic actuator are included in the Fig’s. 2.1a-b configuration in the interests of closing potential “loopholes” that might adversely affect the validity of the Δ_C measurement.

2.4.1 Parameters for proof-of-principle experiment

This subsection more specifically examines representative examples of component and beam parameters as well as occupation value estimates based on those parameters. These representative parameters for the proof-of-principle demonstration are shown in Fig. 2.2.

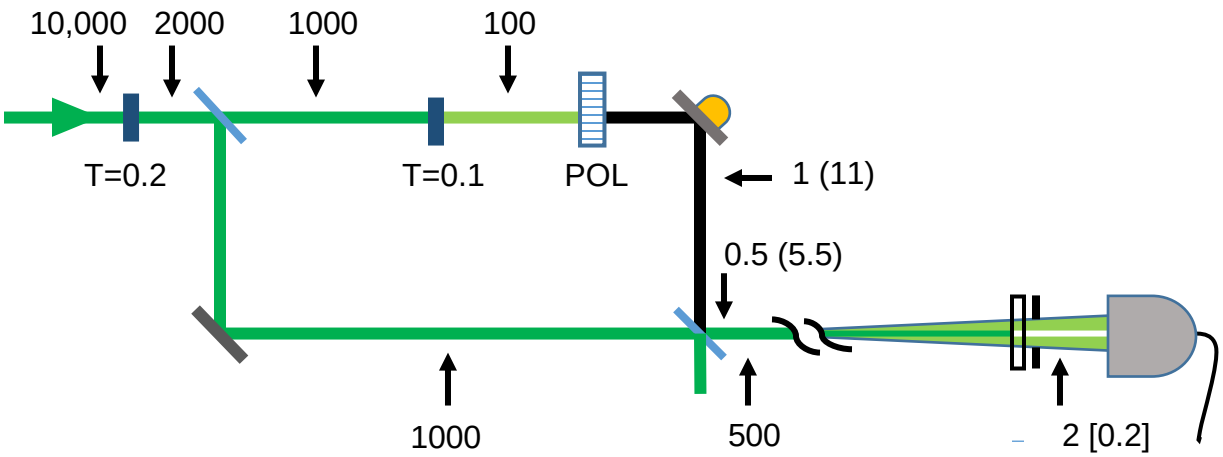

Figure 2.2a. Example of coupled-mode beam power values in micro-Watts and associated probability flux in parentheses for non-ordinary beams. Square bracketed value shows S beam power in uncoupled mode.

An SLM DPPS 532 nm laser provides a 10 mW ~100:1 vertically polarized source beam. The beam is incident on a 0.2 transmissive attenuator Attn-1 and the remaining 2000 μW is incident on a 50:50 beam splitter BS-1. The 1000 μW transmitted by BS-1 is incident on a 0.1 transmissive attenuator Attn-2 leaving 100 μW incident on a 1000:1 extinction value linear polarizer Pol.

Consistent with LR, the 100 μW beam incident beam projects 11% of its intensity or, equivalently, its probability flux, onto the Pol horizontal axis as an empty planar wave, emerging as an empty wave beam with a probability flux of 11 μW-eq.

Because of the 100:1 polarization of the source beam, that 100 μW vertically polarized beam incident on Pol more precisely includes a 1 μW horizontally polarized component beam. Since the utilized polarization axis output of Pol is horizontally oriented, the power (energy flux) of the incident 1 μW horizontally polarized component is fully transmitted as a planar wave in Pol, emerging at the horizontal axis output. Of secondary consequence, that 1 μW incident beam is no longer ordinary upon exiting Pol because its probability flux has fallen from 1 to 0.89 μW-eq, leaving it slightly enriched with an occupation value Ω=1.12. That 0.89 μW-eq probability flux, which

randomly has either an in-phase or an out-of-phase relation with the 11 μW-eq probability flux, is neglected.

An additional output contribution arises from the finite Pol extinction ratio which is >2000:1. As a result a horizontally polarized relatively insignificant <0.05 μW can be neglected relative to the 1 μW on the Pol's horizontal output.

Then the Pol's horizontal output beam resolves to Pwr=1μW and Pwr-eq=11μW-eq which constitutes a moderately depleted pulsed S output beam with an initial occupation value Ω_{Si}= Pwr/Pwr-eq=1μW/11μW-eq=0.09. That moderately depleted pulsed S beam is incident on the mirror of a beam director equipped with a haptic actuator M1-H.

The mirror on M1-H directs the pulsed S beam to a 50:50 beam splitter BS-2. The coupling path of the pulsed S beam and the R restoration beam begins at BS-2. That R beam is derived from the vertically polarized SLM 1000 μW beam fraction reflected off of the first beam splitter BS-1. The R beam encounters a first order 532 nm half wave plate HWP that rotates the beam's polarization state by 90°. The now horizontally polarized 1000 μW R beam is incident on BS-2 coincident with the pulsed S beam spot. The 500 μW fraction of the R beam transmitted by BS-2 is utilized as the R beam on the coupling path. Since the R beam on that path is ordinary, the R beam's probability flux is 500 μW-eq.

Similarly, for the pulsed S beam incident on BS-2, the reflected fraction is utilized as the S beam on the coupling path and consists of pulses with 0.5 μW energy flux (power) and 5.5 μW-eq probability flux. (Time averaged, these values would appear to be half again as large because of the 50% duty cycle of the pulses produced by the chopper wheel.)

Adjustment of the beam director on which BS-2 is mounted provides for concentric collinearity of the S and R beams along the coupling path. In the proximal region of the coupling path where the two beams have comparable Gaussian diameters, the probability flux of the R beam, 500 μW-eq, exceeds that of the S beam pulses, 5.5 μW-eq, by approximately two orders of magnitude. As a result, the two coupled beams in this C-mode configuration are expected to equilibrate to a common final occupation value $\Omega_f=\Omega_{Rf}=\Omega_{Sf}$ over the course of propagating in the proximal region of the coupling path.

That Ω_f is approximately ordinary since the R beam probability flux is much greater than that of the S beam.

As the two beams propagate together into the distal region of the coupling path, the convergent R beam power is progressively concentrated toward the center of the S beam. At the terminus of the coupling path, the 500 μW R beam power is almost entirely blocked by the mask Mk whereas the relative residual R beam power incident as an annular beam on the detector is about two orders of magnitude smaller at ~5 μW. This measurement is acquired by blocking the S beam. Concurrently, with R blocked in U-mode, a still substantial fraction of the S pulse power is incident as an annular beam at ~2 μW which, because of the 50% duty cycle of the pulses, averages as ~1 μW. With both beams present on the coupling path, i.e. C-mode, the S pulse power measured relative to the R beam baseline rises to levels as high as ~20 μW. (The bracketed value [0.2] denotes the S beam power in μW in the uncoupled mode.)

A first order estimate of the initial S beam pulse occupation value Ω_{Si} is readily computed below from the typical beam parameters given here, assuming that the residual R beam is a steady state baseline power and that the S beam pulses are fully restored. A more precise estimate of Ω_{Si} in the absence of those simplifying assumptions, is also be computed to assess the magnitude of the error in the first order estimate.

The U-mode pulse height of ~2 μW=Δ_U constitutes the energy flux of the unrestored annular beam S pulses that are incident on the detector. The C-mode pulse height of ~20 μW= Δ_C. Under the assumption that those pulses are fully restored, Ω_{Sf}=1=Δ_C/Pwr-eq=20 μW/Pwr-eq. The power-equivalent probability flux of the pulses is then Pwr-eq=Δ_C=20 μW, recalling that for an ordinary beam the imposed normalization effectively results in the dimensionless equality of the beam's particle-like (energy) parameter and its complementary wave-like parameter. In the context of normalized, dimensionless irradiance I and intensity W for ordinary beams, I=W=1. This equality can be applied to the presently considered fully restored pulses expressed in Pwr and Pwr-eq units.

Importantly, since the wave-like parameter of a beam does not change in the process of equilibration, the Pwr-eq=Δ_C=20 μW=20 μW-eq determined from the restored pulses is equally applicable to the initial, unrestored pulses.

From this example it can be seen that in general for the first order estimate, Ω_{Si} reduces to the simple ratio of Δ_U and Δ_C,

$\Omega_{Si}=\Delta_U/\Delta_C$.

For the presently considered pulse height measurements where Δ_U~2 μW and Δ_C~20 μW-eq, the first order estimate of the occupation value of the S beam pulses emitted by Pol is Ω_{Si}~0.1. This estimate characterizes the Pol output S pulses as 90% depleted. The principal factor that causes these pulses to be 90% depleted rather than totally depleted, i.e. empty, can be traced to the 100:1 polarization ratio of the SLM source beam.

The accuracy of this first order estimate can be further assessed by removing approximations introduced in that estimate. These approximations specifically relate to the assumption that the pulses are fully restored in C-mode and the assumption that the R beam power lateral to the S pulses correctly represents in the lower level of the Δ_C measurement.

On the coupling path the R beam probability flux is ~500 μW-eq while the S beam pulses are ~5.5 μW-eq. Therefore $\Omega_f\approx0.99$ rather than 1 and the upper level of Δ_C is erroneously ~1% lower than it would have been for total restoration. That error applied to the present example of a ~20 μW pulse height means that the actual upper level of the Δ_C measurement should be increased by ~0.2 μW.

An additional error is related to the depletion of the fraction of the R beam incident on the detector. In the equilibration process the R beam is depleted by the S beam pulse. The respective probability fluxes, 500 μW-eq and 5.5 μW-eq on the coupling path, differ by approximately two orders of magnitude. Consequently, if the initial S beam pulses are substantially depleted, the total power lost by the R beam in the equilibration process is ~5.5 μW. However, because of the R beam's convergence onto the mask, only 5 μW of that beam is incident on the detector giving a faction ~5 μW/500 μW=0.01 of the R beam's probability flux incident on the detector. Therefore the depletion of the R beam incident on the detector is ~0.055 μW during S pulses. Accordingly, the actual power of the R beam during the S pulses is 0.055 μW lower than the measured power level of 5 μW for the ordinary (undepleted) R beam during the times between the S pulses.

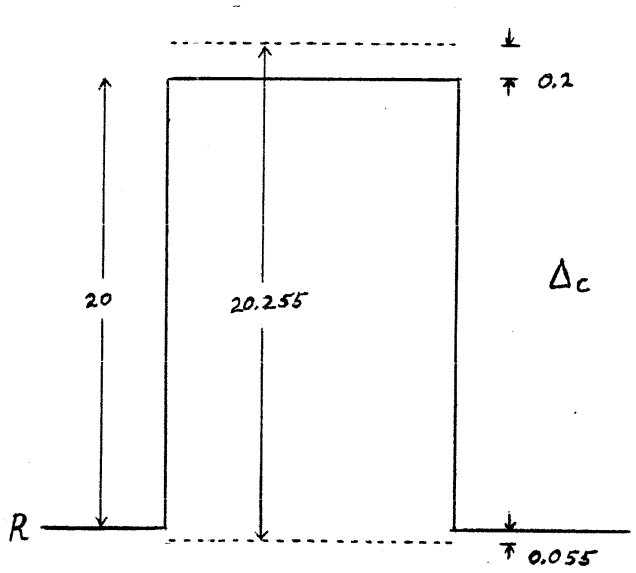

Figure 2.3. Example of a pulse height measurement in coupled mode showing R beam related errors. Numerical values are in microWatts.

For the present example of configuration parameters the combined two errors represent an ~-1% underestimate of the Δ_C measurement and, correspondingly, an ~+1% overestimate of the first order estimate $\Omega_{Si}=\Delta_U/\Delta_C$. These relatively predictable errors associated with the presence of R beam are shown in the Fig. 2.3 diagram of a C-mode pulse. From an experimental perspective, the two measurements, Δ_U and Δ_C, provide an adequately accurate value of Ω_{Si} using only the simple expression $\Omega_{Si}=\Delta_U/\Delta_C$.

As a very important practical matter with regard to potential measurement error, suboptimal alignment of the beams on the coupling path can readily result in partial restoration and an apparent $\Delta_{C\text{-}app}$ that is a large undervalue of the full Δ_C peak height that would otherwise be expected for substantially complete restoration. Consequently, experimental trials acquired with suboptimal alignments typically yield a very wide range of apparent $\Omega_{Si\text{-}app}$ values that can easily far exceed the above ~+1% overestimate of Ω_{Si} associated with the presence of the R beam in C-mode. As alignments are improved, those apparent $\Delta_{C\text{-}app}$ increase and $\Omega_{Si\text{-}app}$ values converge down to the true physical Ω_{Si} value corresponding to substantially complete restoration of the S pulses.

The functional dependence of incomplete restoration on apparent measurement values of $\Delta_{C\text{-}app}$ giving $\Omega_{Si\text{-}app}=\Delta_U/\Delta_{C\text{-}app}$ can be instructively examined by considering several examples. In this exercise an actual initial

value Ω_{Si}=0.1 is assumed. That value is conveniently represented by energy E=0.1 and probability P=1. In terms of $\Omega_{Si}=\Delta_U/\Delta_C$, the unit-less energy measurement values Δ_U=0.1 and Δ_C=1 can be assigned for the actual initial Ω_{Si} where the energy measurement Δ_C=P=1 with complete restoration. However, when restoration is incomplete $\Delta_{C\text{-}app}$ <1 principally as a result of suboptimal alignment.

If the restoration toward ordinary is only 15%, i.e. $\Delta_{C\text{-}app}$=0.15, the apparent measured initial occupation value is $\Omega_{Si\text{-}app}$=0.67 since Δ_U=0.1 is unchanged. In this example, coupling has added only an additional E of 0.05 to the 0.10 already present on the beam. Then the corresponding calculated partially restored final occupation value $\Omega_{Sf\text{-}pr}$=E/P=0.15/1=0.15. Similarly, for 50% restoration, the measured initial occupation value $\Omega_{Si\text{-}app}$=0.2 and the corresponding calculated partially restored final occupation value $\Omega_{Sf\text{-}pr}$=E/P=0.5/1=0.5. For 100% restoration $\Omega_{Si\text{-}app}$= Ω_{Si}=0.1 since $\Omega_{Sf\text{-}pr}$ =1.

From these examples the utility of the apparent measured initial occupation values $\Omega_{Si\text{-}app}=\Delta_U/\Delta_C$ can be appreciated. As incomplete restoration is progressively improved toward complete restoration, the apparent initial occupation value converges down to some minimum that represents the actual initial occupation value, $\Omega_{Si\text{-}app}\rightarrow\Omega_{Si}$.

2.4.2 Results and Discussion

Experimental trials have produced a wide range of $\Omega_{Si\text{-}app}$<1 values. Proper alignment of the beams appears to be the most critical factor in achieving maximum pulse restoration of the presumptively empty wave beam. As alignment is improved, trial values of $\Omega_{Si\text{-}app}$ decrease from values only modestly in the range of <1 to the range of ~0.1. Those trials yielding ~0.1 are postulated to represent the actual Ω_{Si} value that is expected from the 100:1 polarization of the SLM laser.

Importantly however, even for those trials in which pulse restoration is incomplete, any statistically valid experimental trial yielding an $\Omega_{Si\text{-}app}$<1 is potentially evidence in support of the reality of empty waves and evidence in conflict with the probabilistic interpretation of quantum mechanics, PI.

2.4.3 Comments on “equilibration” and “restoration”.

“Equilibration” as applied here is the process in which two separate beams, identified as S and R, are transiently coupled and re-separated. The purpose

of this process is to converge differing occupation values of those respective beams, Ω_S and Ω_R, to a common value Ω. In this process energy quanta, the particle-like aspect of the beams, are transferred from the beam with the higher occupation value to the beam with the lower occupation value. Concurrently, the wave-like aspects of the beams are unchanged in this process.

A particularly useful application of the equilibration process relates to detecting empty or nearly empty waves Ω≈0 at a receiver. Conventional detectability of such waves is achieved by equilibrating those empty waves to an ordinary or near ordinary Ω≈1 state. This application represents a special case of equilibration defined here as “restoration” in which any partially or totally depleted (empty) beam is literally restored to an ordinary state by sufficient acquisition of energy quanta during the coupling. That restoration process is most readily achieved by coupling a depleted or empty beam S with an ordinary beam R, comparable in Gaussian diameter, but with a much higher wave intensity. Because of the very large disparity in the wave intensities of the two beams the final common Ω is only fractionally less than unity.

2.5 ANALOG TO CAPACITORS

The process in which two beams equilibrate to a common Ω as a result of transient coupling is analogous to the process in which two capacitors equilibrate to a common voltage as a result of a transitory parallel coupling of their electrodes. In the fullest sense of this analogy it is most appropriate to consider extrinsic variables for the beams such as probability P, energy E and occupation value Ω in respective relation to the variables of capacitance C, charge Q, and voltage V for the capacitors. The variables for the two beams as well as for the two capacitors are respectively distinguished by the subscripts S and R. The additional subscripts i and f further distinguish the variables where i indicates the initial value of a variable before the transient process occurs and f indicates the final value of a variable after the transient process has been completed.

The fundamental relationship between the beam variables is given by the simple equation Ω=E/P while the analogous fundamental relationship

between the capacitor variables is given by V=Q/C. For the S beam and the R beam the initial fundamental relationships are $\Omega_{Si}=E_{Si}/P_S$ and $\Omega_{Ri}=E_{Ri}/P_R$, respectively. Correspondingly, the final relationships are $\Omega_{Sf}=E_{Sf}/P_S$ and $\Omega_{Rf}=E_{Rf}/P_R$, respectively. For the capacitors, the directly analogous equations are $V_{Si}=Q_{Si}/C_S$, $V_{Ri}=Q_{Ri}/C_R$, $V_{Sf}=Q_{Sf}/C_S$ and $V_{Rf}=Q_{Rf}/C_R$.

For the case of the capacitors, the capacitances C_S and C_R are each invariants that do not change as a result of transient coupling with each other. This invariance is reflected in the lack of i and f subscripts applied in the above equations for those quantities. In that context the capacitances are more properly characterized as “parameters” rather than as “variables”. Conversely, the quantity of charge Q resident on a capacitor can change when that capacitor is coupled to another capacitor and that Q value is appropriately designated as a variable.

This distinction also analogously applies to the beams. The probability P of a beam represents integration of the intrinsic wave intensity (a probability flux density) variable W over the cross section of a propagating beam for some selected time increment $\Delta\tau$. That integration defines the total (extrinsic) probability P of that selected beam segment length. Similarly, the inclusive energy quanta residing on the wave structure of that beam segment is appropriately designated as the total (extrinsic) energy E.

Beam quantities such as the beam intensity W and the irradiance I can also be compared to the capacitor analog since those beam quantities are related to each other by $\Omega=I/W$. However, W and I are intrinsic beam quantities and the analog to capacitors must be applied with care. For a Gaussian beam, specifications of W and I are generally understood to mean the respective maximum values of those quantities which are located at the center of the beam’s Gaussian cross section. If a given beam is divergent, both of those quantities proportionately decrease along the beam path but their ratio I/W remains constant. Consequently, at a more distant point along the beam path, $\Omega=I/W$ is unchanged.

However, if two beams with dissimilar divergences are being considered in a mutual equilibration process, treatment of that equilibration with intrinsic variables at one point along the beam path of the two coupled beams where their Gaussian diameters are similar is not directly relatable to that treatment at a distant point along the beam path where the Gaussian diameters are

dissimilar. That difficulty is avoided when using extrinsic quantities such as P and E which relate to total inclusive probability and energy within a beam segment of some selected length and not to a maximum values of intrinsic quantities that each diminish along a diverging beam.

Then applying the extrinsic E and P to ordinary beams, for which the ordinary occupation value is $\Omega_o=E/P=1$, E=P in dimensionless units, it can be appreciated that the extrinsic parameter of P provides a fixed “capacity” of the beam to hold some energy quantity E under ordinary conditions. Analogously, charging any particular capacitor to some standard reference voltage V_o fixes the value of C based upon the measurable charge Q accumulated on the capacitor since Q=C for that standard voltage V_o.

In the context of the present Fig. 8a proof-of-principle demonstration $0<\Omega_{Si}<<\Omega_{Ri}=\Omega_o=1$ and $E_{Si}<<P_S<<P_R=E_{Ri}$. The corresponding relative proportioned quantities for the capacitor analog are $0<V_{Si}<<V_{Ri}=V_o=1$ and $Q_{Si}<<C_S<<C_R=Q_{Ri}$. For a particular relevant example of the beam-capacitor analog, a similar set of unit-less values is selected: $V_{Si}=0.1$, $Q_{Si}=0.1$, $C_S=1$, $C_R=100$ and $Q_{Ri}=100$.

If the C_S and C_R capacitors with their respective initial charges are equilibrated by transient coupling, the total charge is $Q_T=100.1$ and the total capacitance of the coupled capacitors is $C_T=101$. That results in a common voltage of $V_T=Q_T/C_T=0.9911$ on the coupled C_S and C_R during that transient coupling. If the capacitors are then decoupled, the final voltages on C_S and C_R remain at that common voltage,

$0.9911=V_{Sf}=Q_{Sf}/C_S=V_{Rf}=Q_{Rf}/C_R$

This equation shows that the smaller C_S capacitor, with an initial $V_{Si}=0.1$, has equilibrated almost to the level of the standard reference voltage of $V_o=1$ while the larger C_R capacitor has only fractionally diminished in voltage from its initial $V_o=V_{Ri}=1$. The respective final charges are also from this equation, $Q_{Sf}=0.9911$ and $Q_{Rf}=99.11$.

As a further analogy to the beam restoration process in which only a fraction of the S beam is measured at the detector, the capacitor $C_S=1$ itself can be treated as two smaller parallel-connected capacitors, e.g. $C_{S1}=0.3$ and $C_{S2}=0.7$. Any voltage on C_S is also on C_{S1} and C_{S2}. After the transient coupling is completed, i.e. C_S and C_R have been disconnected, the voltage

of 0.9911 on C_S can be indirectly measured by then disconnecting C_S into separated C_{S1} and C_{S2}, and measuring the voltage on either, e.g. C_{S1}. That voltage measurement on C_{S1} is the same 0.9911 that is present on C_S and completes the capacitor analog to the coupled C-mode beam restoration measurement.

The corresponding uncoupled U-mode capacitor analog measurement follows immediately from the initial C_S parameters V_{Si}=0.1, Q_{Si}=0.1, and C_S=1 since C_R is not coupled to C_S. As a result, the initial C_S variables V_{Si}=0.1 and Q_{Si}=0.1 are also the final variables V_{Sf}=0.1 and Q_{Sf}=0.1. Finally, since the C_{S1} voltage is the same as the C_S voltage, that C_{S1} voltage is also V_{S1f}=0.1, completing the capacitor analog to the coupled U-mode beam restoration measurement.

The above exercise in capacitor equilibration is immediately translatable to beam equilibration by conversion of V, C, and Q to Ω, P, and E respectively. Although the two processes are physically quite distinct, the mathematical computations are essentially identical and the exercise is very instructive in demonstrating that a beam's real wave structure has a "capacity" property for storing energy that is analogous to a capacitor's property for storing charge.

2.7 MODES, WAVE FUNCTIONS AND THEIR INTERACTIONS WITH POLARIZERS

A mode is an electromagnetic radiation coherence wave that may be occupied by one or more energy quanta in which case it would be commonly characterized as a boson state comprised of one or more photons. A mode may have some consequential macroscopic length along its propagation axis such as any of the multiple modes that are simultaneously present in a coherence length of a multi longitudinal mode MLM laser beam. Each mode in a MLM beam is in general occupied by a large multitude of energy quanta. The quanta on any given mode are incrementally different in energy from those of the other modes and the arc bisector orientation of any given mode for an MLM beam, linearly polarized relative to some axis, is that of a random member of a polarization ensemble about that axis. Lasers can also be constructed to emit only a single mode at any given time. The modes of such single longitudinal mode SLM lasers are typically much longer than those of

MLM lasers. However, in common with MLM lasers, the arc bisector orientation of any single mode for an SLM beam linearly polarized relative to some axis is that of a random member of a polarization ensemble about that axis.

Significantly, a source emitting a sequence of linearly polarized discrete photons is functionally analogous to the beam of a linearly polarized SLM laser with respect to the commonality that both sequentially emit single modes and the arc bisectors of those modes have an orientation of a random member of a polarization ensemble referenced to the associated linear polarization axis. This commonality is emphasized at this point because frequent utilization of linearly polarized SLM beams is made here but typically linearly polarized discrete photons are similarly functional albeit with greatly reduced wave intensity and detectable energy quanta. From a representational standpoint that commonality is manifested in a wave function that is generally applicable to linearly polarized SLM beams as well as to linearly polarized discrete photons.

In the context of the present analysis, in which interactions with devices such as polarizers are examined, the convention is followed here of using a compact form of the wave function. However, the notation used in this LR representation of wave functions is deliberately modified from that of PI in the interests of clearly distinguishing objectively real quantities from those of probabilistic quantities.

The analysis begins with an electromagnetic wave mode propagating in free space or in a non-polarized medium. That mode is properly represented by a “pie-vector” amplitude $\underline{\mathbf{\Phi}}$ that is orthogonal to the propagation axis. At any point along the mode’s propagation axis the mode is represented in the transverse plane by an infinite set of equal amplitude radial vectors uniformly distributed over a π/2 arc resulting in a 3-dimensional wave structure of the mode modulated along the propagation axis by the longitudinal wave function ξ. When a pie vector amplitude of the mode is incident on a polarized medium a condensation process occurs that projects the angularly distributed radial vectors onto the polarization axis (or axes) of the polarized medium. These projections result in the 3-dimensional mode condensing to a 2-dimensional mode consisting of a planar wave aligned with the medium’s polarization axis in the transverse plane and modulated along the

propagation axis by the longitudinal wave function ξ. Accordingly, the pie-vector $\underline{\mathbf{\Phi}}$ transitions to a simple vector representation $\mathbf{\Phi}_\delta$ that is aligned to the medium's polarization axis upon entering the medium, orthogonal to the propagation axis and modulated along the propagation axis by the longitudinal wave function ξ. The δ subscript denotes that $\mathbf{\Phi}_\delta$ is a planar wave condensed from a pie-vector $\underline{\mathbf{\Phi}}$ in a process analogous to a Dirac-delta function. In treating transitions between pie-vectors to vectors it is mathematically more expedient to utilize a vector form $\mathbf{\Phi}$ that serves as equivalency vector substitute for the pie vector $\underline{\mathbf{\Phi}}$. The requisite properties of the equivalency vector $\mathbf{\Phi}$ can readily be determined by considering a $\underline{\mathbf{\Phi}} \rightarrow \mathbf{\Phi}_\delta$ transition and imposing conservation of probability.

The pie vector form wave function representing a free space mode is

$$\underline{\mathbf{\Phi}}(\theta,z,t)=\xi(z,t)\, m\, \underline{\mathbf{r}}(\theta).$$

The pie vector $\underline{\mathbf{r}}(\theta)$ is a unit modulus, $|\underline{\mathbf{r}}(\theta)|=1$, transverse representation of $\underline{\mathbf{\Phi}}(\theta)$ comprised of an infinite set of equal amplitude unit magnitude radial vectors uniformly distributed over a π/2 arc with an arc bisector at θ. The longitudinal wave function is assigned a unit modulus, $|\xi|=1$, so that the magnitude of $\underline{\mathbf{\Phi}}(\theta)$ is subsumed in some scalar coefficient m. The orientation θ denotes the objectively real bisector of the $\underline{\mathbf{\Phi}}(\theta)$ arc span.

The particular example of θ=0° is first examined before proceeding to a general case of θ. When an objectively real $\underline{\mathbf{\Phi}}(0°)$ is normally incident on a polarizer such as calcite that has a polarization axis at 0°, the cosine projections of the $\underline{\mathbf{r}}(0°)$ unit magnitude radial vectors along the 0° axis integrated over ±π/4 introduces a factor of $\sqrt{2}$ which, divided by π/2, gives an average projection of almost exactly 0.9. More significantly, however, as the projective process proceeds, the resultant entity arising from the vector sum of the radial vector cosine projections is a very narrow, large amplitude peak trivially centered at 0° by symmetry in a physical process mathematically analogous to the Dirac delta function.

Physically in that process of $\underline{\mathbf{\Phi}}(0°) \rightarrow \mathbf{\Phi}_\delta(0°)$, probability is conserved consistent with the Dirac delta function applied to the squared modulus of a spatially extended amplitude condensing into a vanishingly narrow peak. The wave function of $\mathbf{\Phi}_\delta(0°)$ is represented by

$$\mathbf{\Phi}_\delta(0°)=\xi\, M\, \mathbf{r}_\delta(0°)$$

where δ subscripts explicitly denote the vector quantities $\mathbf{\Phi}_\delta$ and $\mathbf{r}_\delta$ as physically planar condensations in the transverse plane. M is the scalar magnitude of the $\mathbf{\Phi}_\delta$ vector amplitude.

In analyzing transitions of amplitudes into and out of polarizers it is mathematically more expeditious if all amplitudes can be expressed in vector form. To this end, the "equivalency vector" $\mathbf{\Phi}$ is introduced here in mathematical replacement of the pie vector $\underline{\mathbf{\Phi}}$ which more accurately physically represents modes in free space and in non-polarized mediums.

Nevertheless, the equivalency vector $\mathbf{\Phi}$ still retains the properties necessary to represent mode interactions with polarizers while properly conserving probability in those interactions.

In contrast to the pie vector,

$\underline{\mathbf{\Phi}}(0°)=\xi\, m\, \underline{\mathbf{r}}(0°)$

where its arc bisector unit vector is oriented at 0° in the transverse plane

the equivalency vector

$\mathbf{\Phi}(0°)=\xi\, M'\, \mathbf{r}(0°)$

is represented in the transverse plane by a unit radial vector **r** oriented at **0°** and that vector is scaled by a magnitude M′.

In these respects the equivalency vector amplitude is structurally similar to the mode vector amplitude within a polarizer,

$\mathbf{\Phi}_\delta(0°)=\xi\, M\, \mathbf{r}_\delta(0°)$

where 0° is necessarily the orientation of the polarization axis of the polarizer in which $\mathbf{\Phi}_\delta(0°)$ is propagating. For the equivalency vector $\mathbf{\Phi}(0°)$, that δ subscript is omitted as a reminder that the equivalency vector is not physically a planar condensate but is instead a mathematical substitute for the polarizer-incident pie vector $\underline{\mathbf{\Phi}}(0°)$.

The mathematical functionality of that substitution is made possible by the probability conservation in the $\underline{\mathbf{\Phi}}(0°) \rightarrow \mathbf{\Phi}_\delta(0°)$ transition which allows, in a time reversal process, the imposition of the same magnitude onto the equivalency wave function $\mathbf{\Phi}(0°)$ as that on the planar wave function $\mathbf{\Phi}_\delta(0°)$

propagating within the polarizer, i.e. M′=M. Mathematically this imposes the probability of the pie vector $\underline{\mathbf{\Phi}}(0°)$ onto the equivalency vector $\mathbf{\Phi}(0°)$.

The above special case of θ=0° for modes incident on a polarizer can readily be extended to the general case of some objectively real θ for the pie vector arc bisector orientation. For a pie vector with an arc bisector at θ, the vector sum of the radial vectors is by symmetry a resultant vector oriented at θ.

This allows a decomposition of an equivalency vector amplitude

$$\mathbf{\Phi}(\theta)=\mathbf{\Phi}(0°)\cos\theta + \mathbf{\Phi}(90°)\sin\theta$$

$$=\xi M\cos\theta\,\mathbf{r}(0°) + \xi M\sin\theta\,\mathbf{r}(90°).$$

We then consider the above decomposed vector amplitude incident on a two channel polarizer such as calcite where the “vertical” polarization axis is at 0° and the “horizontal” polarization axis is at 90°. Specifically, the equivalency vectors $\mathbf{\Phi}(0°)\cos\theta$ and $\mathbf{\Phi}(90°)\sin\theta$ are incident respectively on the polarizer’s 0° and 90° axes. As a result, the δ-form amplitudes

$$\mathbf{\Phi}_\delta(0°)=\xi M\cos\theta\,\mathbf{r}_\delta(0°)$$

and

$$\mathbf{\Phi}_\delta(90°)=\xi M\sin\theta\,\mathbf{r}_\delta(90°)$$

respectively propagate on the 0° and 90° polarization channels. The squared moduli of these two δ-form amplitudes confirms that probability is conserved in this representation and demonstrates the utility of employing the equivalency vector in place of the pie vector for the general case of a θ arc bisector.

Summary of Notation:

$\underline{\mathbf{\Phi}}(\theta)$ and $\underline{\mathbf{r}}(\theta)$ are pie vectors that geometrically and mathematically correspond to modes in free space.

$\mathbf{\Phi}(\theta)$ and $\mathbf{r}(\theta)$ are “equivalency” vectors that generally can be used as simplified mathematical vector substitutes for pie vector representations of modes in free space.

$\mathbf{\Phi}_\delta(\theta)$ and $\mathbf{r}_\delta(\theta)$ are vector quantities that geometrically and mathematically correspond to δ-form modes in polarizers.

The outcome of energy quanta on modes incident on polarizers must also be addressed in the context of the wave functions.

QuWT

The transfer of energy quanta of the mode onto a channel of a polarizer is deterministically dependent upon the intersection of the mode's incident arc intersecting that channel. That condition is determined from the equivalency vector orientation θ. If

$-45° < \theta < +45°$

the arc intersects the 0° vertical polarization axis and the energy quanta that occupy the mode are confined to the vertical polarization channel of the polarizer as the radial vectors of the mode projectively condense along the vertical polarization axis. Conversely if

$+45° < \theta < +135°$

the energy quanta are confined to the polarizer's horizontal polarization channel.

The presence of energy quanta on a mode amplitude is indicated by a "+" subscript. For example, the equivalency vector amplitude

$$\mathbf{\Phi}(\theta)_{+} = \xi M \mathbf{r}_{\delta}(\theta)_{+} = \xi \mathbf{r}(\theta)_{+}$$

is occupied and has a unit modulus since M=1. If $-45° < \theta < +45°$ and $\mathbf{\Phi}(\theta)_{+}$ is incident on a calcite polarizer, the projection of that amplitude onto the vertical polarization axis results in a occupied vector amplitude

$$\mathbf{\Phi}_{\delta}(0°)_{+} = \xi \cos\theta \, \mathbf{r}_{\delta}(0°)_{+}$$

propagating on the vertical polarization channel with a magnitude $\cos\theta$. Then, deterministically,

$$\mathbf{\Phi}_{\delta}(90°) = \xi \sin\theta \, \mathbf{r}_{\delta}(90°)$$

is the vector amplitude propagating on the horizontal polarization channel with a magnitude $|\sin\theta|$. Since $-45° < \theta < +45°$, the associated arc of the incident mode does not intersect the horizontal axis and the vector amplitude propagating on the horizontal polarization channel $\mathbf{\Phi}_{\delta}(90°)$ is an "empty" wave mode as indicated by the absence of a "+" subscript.

There are numerous occasions encountered in the analyses below in which an incident mode is polarized about some specified polarization axis where that axis has an orientation θ as distinct from specifying that the objectively real incident mode itself has some specified orientation. That distinction is

addressed here by adopting the convention that θ_α denotes the orientation of a mode that has the orientation of a random member α of a polarization ensemble centered about θ. The subscript is given by a lower case Greek letter other than δ to avoid confusion with δ-form modes.

For example, the notation $0°_\alpha$ specifies that the amplitude is transversely represented by the orientation θ (bisector angle) of a random member α of the 0°-polarization ensemble. θ is in the range from -45° to +45° with a frequency distribution determined by the ensemble's cosine squared curvilinear envelope. This convention can be instructively visualized using the finite 16-member ensemble depicted in FIG. 2.4 where α is some random value from 1→16 and θ is the bisector angle of that α member.

An expression for the bisector orientation of a given α member can readily be computed. For the finite 16-member vertical polarization-ensemble in radians

$$0_\alpha=\cos^{-1}[(\alpha-1)/15]^{1/2}-\pi/4$$

The presence of an energy quantum on a discrete "photon" wave packet or of (a large number of) energy quanta on a mode is denoted by an appended subscript "+".

It is important to emphasize that any successive input mode, similarly represented by an amplitude $\underline{\mathbf{\Phi}}_1(0°_\alpha)$, has a realized random member α orientation that is uncorrelated to the realized random member α orientation of any of the temporally preceding modes. This property is noted here because in the course of this analysis, there arise circumstances in which two or more simultaneously present amplitudes having random orientations interact with each other. For these simultaneously present amplitudes, the convention applied in this disclosure is that the amplitudes have mutually non-correlated random orientations when their Greek letter indices are respectively different and have mutually correlated random orientations when those indices are respectively the same.

If incident modes are "vertically" polarized, in LR that implies that the orientation θ of the mode is statistically that of a random member of a vertical polarization ensemble as depicted in Fig. 2.4 using a finite-member ensemble for instructional purposes.

If the source directs these linearly polarized modes at a two-channel polarizer where the polarization axis of the ensemble is in alignment with one of the polarization axes of the polarizer, e.g. its vertical axis, then an individual source mode has an orientation $0°_{\alpha}$ where α is some random number 1 to 16. The present axial alignment has important consequences. From Fig. 2.4, the arcs of all of the ensemble member modes intersect the polarizer's vertical polarization axis. As a result for any particular mode of those 16 the energy quanta on the mode transitions onto the vertical channel of the polarizer along with the cosine projection of the incident mode amplitude. That incident amplitude from the source is

$$\mathbf{\Phi}(0°_{\alpha})_{+}=\xi\,\mathbf{r}(0°_{\alpha})_{+}$$

which is normalized to a unit modulus since the magnitude M=1. The amplitude in the polarizer's vertical channel is

$$\mathbf{\Phi}_{\delta}(0°)_{+}=\xi\cos(0°_{\alpha})\;\mathbf{r}_{\delta}(0°)_{+}$$

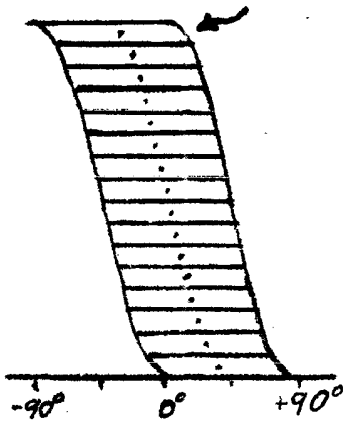

Fig. 2.4. A graphical representation of a 0°-polarized ensemble of modes, showing here for instructional purposes a finite 16-member ensemble. Each member (row) represents an ordinary mode with a transverse arc span of 90°. The arc bisectors of each member, denoted by arc-centered dots, are in a statistical cosine squared distribution about 0°. The notation $0°_{\alpha}$ specifies a mode that has the bisector orientation of a random member α of a 0°-polarized ensemble. For the illustrated ensemble, the members are designated by α=1→16.

that retains the energy quanta that had resided on the incident $\mathbf{\Phi}(0°_{\alpha})_{+}$ but has a reduced wave amplitude as a result of the cosine projection of the α mode onto the polarizer's vertical axis. Concurrently the amplitude on the polarizer's horizontal channel

$\mathbf{\Phi}_{\delta}(90°)=\xi \sin(0°_{\alpha})\ \mathbf{r}_{\delta}(90°)$

has none of the energy quanta that had resided on the incident $\mathbf{\Phi}(0°_{\alpha})_{+}$. That empty wave amplitude has a magnitude $|\sin(0°_{\alpha})|$ as a result of the sine projection of the α mode onto the polarizer's horizontal axis.

2.8 QUANTUM LOOP CALCULATIONS

Quantum loops present quintessential examples demonstrating the phenomenon of non-local superposition from the perspective of "the Probabilistic Interpretation" of the underlying quantum mechanical formalism, PI. That phenomenon is often cited by PI as refutation of local realism.

The electromagnetic wave functions for two different loops are analyzed here from the perspective of LR. These loops are a pair of contiguous oppositely oriented calcite crystals as illustrated in Fig. 2.5 and a polarizing beam splitter Mach-Zehnder Loop, PBS M-Z Loop, as illustrated in Fig. 2.6a. From the perspective of the Probabilistic Interpretation of quantum mechanics, PI, the quantum state of a mode to either loop input is exactly duplicated at the loop output in a process then identified as "unitary."

2.8.1 Mode transit of a calcite loop

The loop analysis begins with the Fig. 2.5 calcite loop, a pair of contiguous, oppositely oriented calcite polarizers. In this and in subsequent analyses the amplitudes are subscripted with the number of the path segment on which they reside since different path segments may be associated with wave function state transitions.

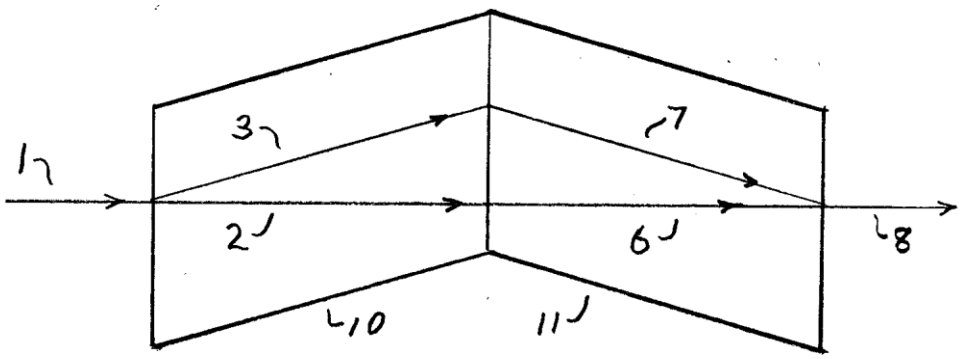

Fig. 2.5 Diagram of a calcite loop.

The (unit modulus) amplitude incident on path **1** is

$\mathbf{\Phi}_1(\theta)_+ = \xi\, \mathbf{r}(\theta)_+$

where $-45° < \theta < +45°$ without loss of generality since analysis with the orthogonal condition is straightforward.

The orientation θ of $\mathbf{\Phi}_1(\theta)$ may be some random value in a uniform distribution from −45° to +45°. Alternatively, $\mathbf{\Phi}_1(\theta)$ may be identified as derived from a 0°-linearly polarized source. In that case θ is still in the range from −45° to +45° but is then derived from a statistical cosine squared distribution and the incident amplitude's orientation could be more precisely characterized as some $0°_\mu$ rather than θ. However, in the following analyses below the original distribution associated with the orientation θ of the incident $\mathbf{\Phi}_1$ is not generally of consequence and it is more appropriate to simply identify the orientation as some objectively real θ within a range such as −45° to +45°.

Continuing onto path **2**, the amplitude

$\mathbf{\Phi}_{\delta 2}(0°)_+ = \xi \cos\theta\, \mathbf{r}_\delta(0°)_+$

is a δ-form planar wave mode because it is propagating inside a polarized media. $\mathbf{\Phi}_{\delta 2}$ retains the energy quanta that had been on $\mathbf{\Phi}_1(\theta)_+$ because the

transverse arc for that θ bisector orientation intersected the 0° polarization axis of calcite **10**.

For path **6** the amplitude

$\mathbf{\Phi}_{\delta 6}(0°)_{+}=\mathbf{\Phi}_{\delta 2}(0°)_{+}$

Resulting in

$\mathbf{\Phi}_{\delta 6}(0°)_{+}= \xi \cos\theta\, \mathbf{r}_{\delta}(0°)_{+}$

since calcites **10** and **11** are contiguous and there is no amplitude transition in the passage from the vertical 0° polarization channel on calcite **10** to that on calcite **11**.

The path **3** amplitude

$\mathbf{\Phi}_{\delta 3}(90°)=\xi \sin\theta\, \mathbf{r}_{\delta}(90°)$

is the complementary horizontal axis projection of the incident amplitude. $\mathbf{\Phi}_{\delta 3}$ is an empty wave mode because of the orientation constraint $-45°<\theta<+45°$ on θ. In analogy to the $\mathbf{\Phi}_{\delta 2}(0°)_{+}$, $\mathbf{\Phi}_{\delta 6}(0°)_{+}$ equivalence the amplitude on path **7** is

$\mathbf{\Phi}_{\delta 7}(90°)=\xi \sin\theta\, \mathbf{r}_{\delta}(90°)$.

With in-phase conditions present for the two orthogonal amplitudes converging to the output face of calcite **11**, the vector sum of

$$\mathbf{\Phi}_{\delta 6}(0°)_{+}+\mathbf{\Phi}_{\delta 7}(90°)=\xi\,[\cos\theta\, \mathbf{r}_{\delta}(0°)_{+}+ \sin\theta\, \mathbf{r}_{\delta}(90°)]$$

$$=\xi\, \mathbf{r}(\theta)_{+}$$

$$=\mathbf{\Phi}_{8}(\theta)_{+}$$

$$=\mathbf{\Phi}_{1}(\theta)_{+}. \qquad .$$

This conjuncture at the calcite **11** exit face results in a loop output mode, second line above, identical to the input mode consistent with the unitary property of the calcite loop required by the underlying quantum formalism. However, this LR representation does not impose the non-local superposition necessitated when the loop transit is represented by PI.

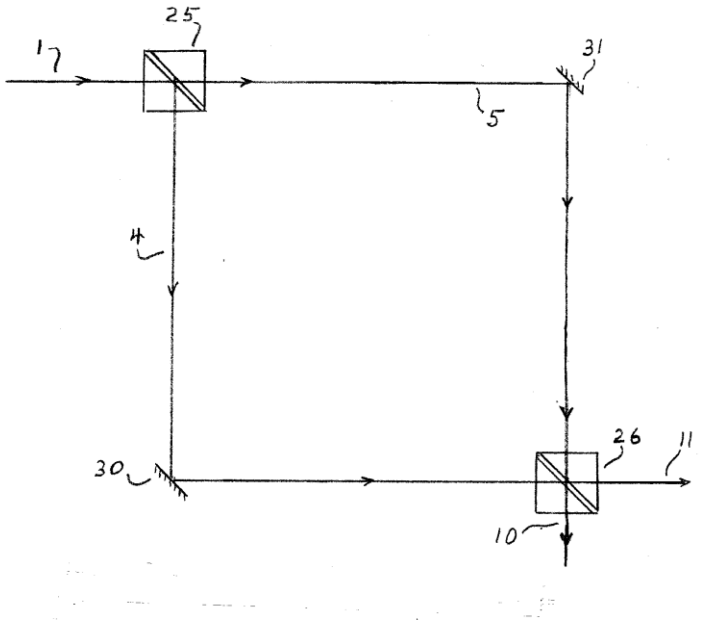

Fig. 2.6. A polarizing beam splitter Mach-Zehnder, PBS M-Z loop.

2.8.2 Mode transit of a PBS M-Z loop

Fig. 2.6a illustrates a polarizing beam splitter Mach-Zehnder loop. Consistent with the underlying quantum formalism, transit of this loop is unitary as is transit of a calcite loop. The LR analysis of mode transit of the PBS M-Z loop is more involved than that of the calcite loop but is nevertheless straightforward. In common with the LR transit analysis of the calcite loop, the LR transit analysis of the PBS M-Z loop does not impose the non-local superposition necessitated when the loop transit is represented by PI. From an LR perspective, the PBS M-Z loop configuration is of particular interest because of the opportunities presented by the spatial separation of the two constituent polarizers.

In the LR analysis of the PBS M-Z loop, the mode's arc bisector orientation θ is constrained to $-45° < \theta < +45°$ on the incident mode

$\mathbf{\Phi}_1(\theta)_+ = \xi\, \mathbf{r}(\theta)_+$.

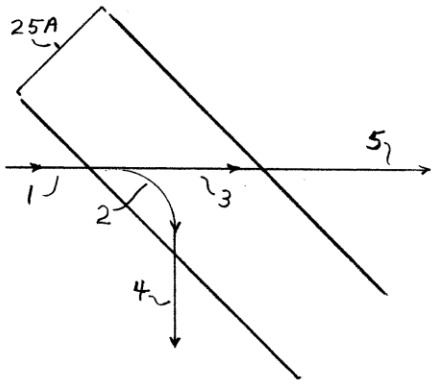

Fig. 2.6b. A diagrammatic representation of an incident non-planar mode on path 1 projectively condensing in the PBS dielectric layer 25A to a vertically oriented delta-form planar wave on path 2 and to a horizontally oriented delta-form planar wave on path 3. Those planar waves emerge from 25A to form non-planar modes that that have the orientations of random members of vertical and horizontal polarization ensembles, respectively.

The delta-form projections of $\Phi_1(\theta)_+$ inside the PBS **25** dielectric layers, as shown in **25A** of Fig. 2.6b are

$$\mathbf{\Phi}_{\delta 2}(0°)_+ = \xi \cos(\theta)\mathbf{r}_{\delta}(0°)_+$$

and

$$\mathbf{\Phi}_{\delta 3}(90°) = \xi \sin(\theta)\mathbf{r}_{\delta}(90°).$$

In a statistical emission process these amplitudes respectively produce

$$\mathbf{\Phi}_4(0°_{\alpha})_+ = \xi \cos(\theta)\mathbf{r}(0°_{\alpha})_+$$

and

$$\mathbf{\Phi}_5(0°_{\alpha} + 90°) = \mathbf{\Phi}_5(90°_{\alpha})$$

$$= \xi \sin(\theta)\mathbf{r}(90°_{\alpha}).$$

This statistical emission process occurs at the output of a polarizer when an exit wave is unaccompanied by an orthogonal exit wave.

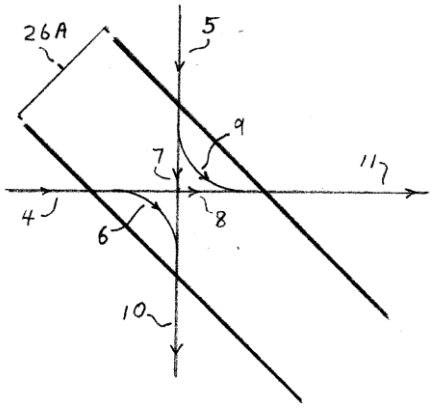

Fig. 2.6c. Diagrammatic representation of waves on paths 4 and 5 entering the dielectric layer 26A of PBS 26 as interacting planar delta-form waves that exit 26A as non-planar waves on paths 10 and 11. Notably, the orientations of those non-planar waves are deterministically set by the conjunction of the orthogonal planar waves from which they are formed.

After reflections at mirrors **30** and **31** the respective projections of $\mathbf{\Phi}_4(0°_\alpha)_+$ and $\mathbf{\Phi}_5(90°_\alpha)$ inside the PBS **26** dielectric layers **26A** are the δ-forms

$$\mathbf{\Phi}_{\delta 6}(0°)_+ = \xi\cos(\theta)\cos(0°_\alpha)\mathbf{r}_\delta(0°)_+ ,$$

$$\mathbf{\Phi}_{\delta 7}(90°) = \xi\sin(\theta)\sin(90°_\alpha)\mathbf{r}_\delta(90°)$$

$$= \xi\sin(\theta)\cos(0°_\alpha)\mathbf{r}_\delta(90°),$$

$$\mathbf{\Phi}_{\delta 8}(0°) = \xi\cos(\theta)\sin(0°_\alpha)\mathbf{r}_\delta(0°),$$

and

$$\mathbf{\Phi}_{\delta 9}(90°) = \xi\sin(\theta)\sin(0°_\alpha)\mathbf{r}_\delta(90°).$$

The δ-form projections $\mathbf{\Phi}_{\delta 6}(0°)_+$ and $\mathbf{\Phi}_{\delta 7}(90°)$ sum vectorally to give a resultant on path **10**, Fig.'s **2A** and **2C**

$$\mathbf{\Phi}_{\delta 6}(0°)_+ + \mathbf{\Phi}_{\delta 7}(90°) = \xi\cos(\theta)\cos(0°_\alpha)\mathbf{r}_\delta(0°)_+ + \xi\sin(\theta)\cos(0°_\alpha)\mathbf{r}_\delta(90°)$$

$$= \xi\cos(0°_\alpha)[\cos(\theta)\,\mathbf{r}_\delta(0°)_+ + \sin(\theta)\mathbf{r}_\delta(90°)]$$

$$= \xi\cos(0°_\alpha)\mathbf{r}(\theta)_+$$

$$= \mathbf{\Phi}_{10}(\theta)_+.$$

The line 2→3 transition of the bracketed [ ] factor to $\mathbf{r}(\theta)_+$ represents a non-random emission process in which orthogonal, mutually accompanying waves $\mathbf{\Phi}_{\delta 6}(0°)_+$ and $\mathbf{\Phi}_{\delta 7}(90°)$ deterministically combine to a definite orientation.

Similarly, the δ-form projections $\mathbf{\Phi}_{\delta 8}(0°)$ and $\mathbf{\Phi}_{\delta 9}(90°)$ sum vectorally to give a resultant on path **11**

$$\mathbf{\Phi}_{\delta 8}(0°)+\mathbf{\Phi}_{\delta 9}(90°)=\xi\cos(\theta)\sin(0°_\alpha)\mathbf{r}_\delta(0°)+\xi\sin(\theta)\sin(0°_\alpha)\mathbf{r}_\delta(90°).$$

$$=\xi\sin(0°_\alpha)[\cos(\theta)\mathbf{r}_\delta(0°)+\sin(\theta)\mathbf{r}_\delta(90°)]$$

.
$$=\xi\sin(0°_\alpha)\mathbf{r}_\delta(\theta)$$

$$=\mathbf{\Phi}_{11}(\theta).$$

The LR analysis of the PBS loop demonstrates that the $\mathbf{\Phi}_{10}$ and $\mathbf{\Phi}_{11}$ orientations are identical to that of $\mathbf{\Phi}_1$. Moreover, $|\mathbf{\Phi}_{10}|^2+|\mathbf{\Phi}_{11}|^2$ shows that probability is conserved relative to $|\mathbf{\Phi}_1|^2$. $\mathbf{\Phi}_{10}(\theta)_+$ is occupied and $\mathbf{\Phi}_{11}(\theta)$ is empty.

OUTCOME WHEN PATH 5 OF PBS M-Z LOOP IS BLOCKED

It is of particular interest at this juncture to examine the resultant output loop amplitudes $\mathbf{\Phi}_{10}$ and $\mathbf{\Phi}_{11}$ when path **5** is blocked and the empty $\mathbf{\Phi}_5$

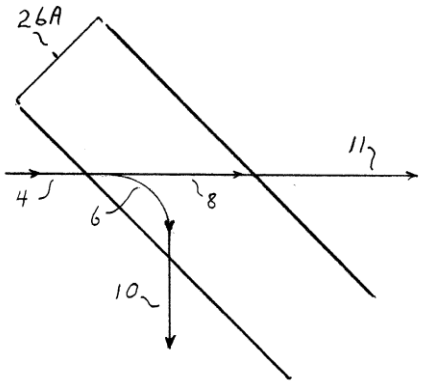

Fig. 2.6d. Diagrammatic representation of waves on dielectric 26A when path 5 of the PBS M-Z loop is blocked.

does not reach PBS **26**. With that blockage, at PBS **26** the result is similar to $\mathbf{\Phi}_1$ incident on PBS **25** yielding $\mathbf{\Phi}_4$ and $\mathbf{\Phi}_5$. With path 5 blocked we have only

the $\mathbf{\Phi}_6$ and $\mathbf{\Phi}_8$ δ-form amplitudes to consider in the PBS 26 dielectric layer shown as **26A** in Fig. 2.6d. We have again in **26A**

$\mathbf{\Phi}_{\delta 6}(0°)_+ = \xi \cos(\theta)\cos(0°_\alpha)\mathbf{r}_\delta(0°)_+$.

In an emission process

$\mathbf{\Phi}_{10}(0°_\beta)_+ = \xi \cos(\theta)\cos(0°_\alpha)\mathbf{r}(0°_\beta)_+$.

Similarly,

$\mathbf{\Phi}_8(0°)_+ = \xi \cos(\theta)\sin(0°_\alpha)\mathbf{r}_\delta(0°)$

yields, in an emission process,

$\mathbf{\Phi}_{11}(90°_\beta) = \xi \cos(\theta)\sin(0°_\alpha)\mathbf{r}(90°_\beta)$.

With path **5** blocked, the resultant $\mathbf{\Phi}_{10}(0°_\beta)_+$ and $\mathbf{\Phi}_{11}(90°_\beta)$ have the orientations of random members of 0°-polarized and 90°-polarized ensembles, respectively, but correlated to the β member of those ensembles. With respect to the occupied output path $\mathbf{\Phi}_{10}$, the two conditions of an unblocked and a blocked path **5** respectively yield different outcomes

$\mathbf{\Phi}_{10}(\theta)_+ = \xi \cos(0°_\alpha)\mathbf{r}(\theta)_+$

and

$\mathbf{\Phi}_{10}(0°_\beta)_+ = \xi \cos(\theta)\cos(0°_\alpha)\mathbf{r}(0°_\beta)_+$.

2.9 INTERACTION-FREE MEASUREMENT

Totally interaction-free measurement IFM can be implemented by modifying the Fig. 2.6a PBS M-Z loop to the configuration depicted in Fig. 2.7. The IFM relates to an object **20** that potentially is either absent, leaving path **5** unblocked, or present, causing path **5** to be blocked.

The functionality of the Fig. 2.7 configuration necessitates the path **1** $\mathbf{\Phi}_1(\theta)_+$ be multi-photon linearly polarized modes with respect to the vertical 0° axis. A beam splitter **35** extracts a photon-occupied sample of the incident modes, identified as $\mathbf{\Phi}_{1B}(\theta)_+$ and directs it on path **1B** to a polarizer **17** leaving the normalized remainder $\mathbf{\Phi}_{1A}(\theta)_+ = \xi\,\mathbf{r}(\theta)_+$ incident on path **1A**. Concurrently, the $\mathbf{\Phi}_{10}(\theta)_+$ mode, temporally derived from the same incident $\mathbf{\Phi}_1(\theta)_+$ mode as $\mathbf{\Phi}_{1B}(\theta)_+$ by path equalization, encounters a polarizer **15**. Polarizers **17** and **15** are both set to +45° with the two polarizers followed by detectors **18** and **16**,

respectively. The detector outputs are connected to a coincidence module **19**.

If object **20** is absent, path **5** is unblocked and $\mathbf{\Phi}_{10}$ arrives at polarizer **15** as

$$\mathbf{\Phi}_{10}(\theta)_{+}=\xi\cos(0°_{\alpha})\mathbf{r}(\theta)_{+}$$

$$=\xi\cos(0°_{\alpha})\mathbf{r}(0°_{\mu})_{+}$$

where in the particular present case it is consequential that the orientation θ can be expressed as $\theta=0°_{\mu}$, i.e. as the orientation of a random member of a 0°-polarization ensemble.

Thereby, for a large number of successive modes arriving at the Fig. 2.7 configuration, 50% register as coincidences at module **19** and 50% are null events with neither detector contributing a positive signal to module **19**. There are no single events in which coincidence module **19** receives a positive signal from only one of the two detectors for a given mode incident on the Fig. 2.7 configuration.

Alternatively, if object **20** is present, path **5** is blocked and $\mathbf{\Phi}_{10}$ arrives at polarizer **15** as

$$\mathbf{\Phi}_{10}(0°_{\beta})_{+}=\xi\cos(\theta)\cos(0°_{\alpha})\mathbf{r}(0°_{\beta})_{+}$$

and the 0°-polarization ensemble member orientations $0°_{\beta}$ of $\mathbf{\Phi}_{10}$ and $0°_{\mu}$ of $\mathbf{\Phi}_{1B}$ are mutually uncorrelated.

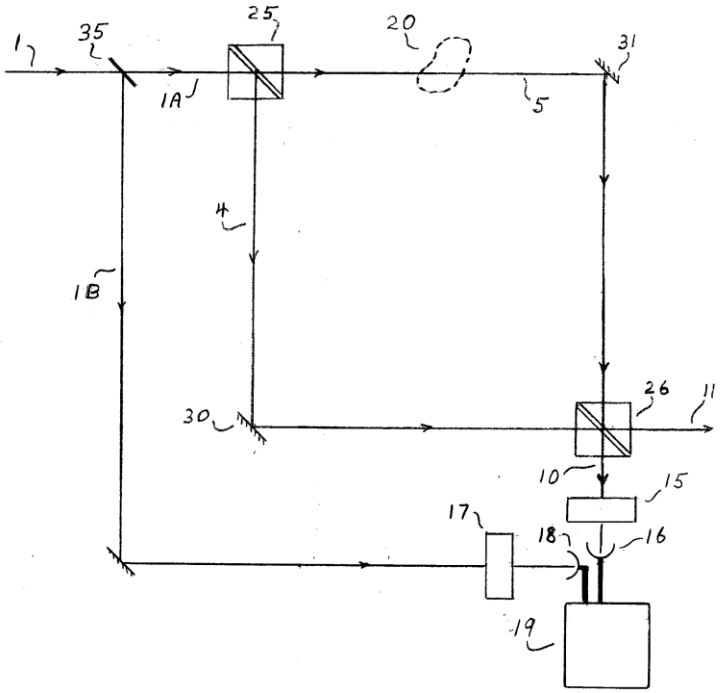

Fig. 2.7. 100% interaction-free measurement, IFM, with a vertically polarized SLM source and a modified PBS M-Z loop.

Consequently, as a large number of successive modes are incident on the Fig. 2.7 configuration, the coincidence module **19** registers 25% coincident events, 50% single events and 25% null events.

The differing measurement results of the coincidence module **19** permit a determination of whether **20** is either absent or present. In principle, the presence of object **20** is established with certainty as soon as a first single event is measured. Most notably the Fig. 2.7 configuration can determine the presence of object **20** with100% efficient interaction-free measurement.